The response of a capacitively coupled discharge to the formation of dust particles: Experiments and modeling

I. Denysenko[a)]
School of Physics and Technology, V. N. Karazin Kharkiv National University, Svobody sq. 4, 61077 Kharkiv, Ukraine

J. Berndt and E. Kovacevic
Institute of Experimental Physics II, Ruhr-University Bochum, D-44780 Bochum, Germany

I. Stefanovic
Institute of Experimental Physics II, Ruhr-University Bochum, D-44780 Bochum, Germany and Institute of Physics, POB 57, 11001 Belgrade, Serbia and Montenegro

V. Selenin and J. Winter
Institute of Experimental Physics II, Ruhr-University Bochum, D-44780 Bochum, Germany

(Received 17 March 2006; accepted 21 June 2006; published online 26 July 2006)

The influence of dust particles on the properties of a capacitively coupled $Ar-C_2H_2$ discharge is studied both experimentally and theoretically. The results of measurements of the intensity and spatial distribution of the emitted light, the line width of the fast component of H_α line and of the electron density during the particle growth are presented. To analyze the experimental results a one-dimensional discharge model is developed. Using the model the effects of dust grains on the power absorption (taking into account stochastic and Ohmic heating in the plasma sheaths), the optical emission intensity profile, the sheath size, the rf electric field and on the energy of positive ions bombarding the electrodes are investigated. In particular, it is shown that the decrease of the power absorption in the sheaths of complex plasmas is due to the dependence of the stochastic and Ohmic heating in the plasma sheaths on the electron temperature and the current flowing across the discharge plates. The results of the calculations are compared with the available experimental data and found to be in good agreement. © *2006 American Institute of Physics*.
[DOI: 10.1063/1.2222258]

I. INTRODUCTION

Complex plasmas (i.e., plasmas containing electrons, positively and negatively charged ions and nanometer—or even micrometer—sized particles) are of great interest for many technological applications, especially in the development of novel nanomaterials.[1,2] Nanoparticles (dust grains) can severely reduce the yield and performance of fabricated devices for microelectronic industry, whereas in some technologies their presence in the plasma environment is desired and useful.[3] They are becoming, for example, more and more indispensable in the modern technology of composite materials, in the fabrication of hard coatings[4] and silicon films.[5,6] Moreover, the processing of externally injected particles into the plasma can yield unique objects, like coated or layered grains with desired surface structures.

One of the most important aspects of dusty plasmas concerns the fact that the presence of particles strongly affects the discharge characteristics.[7] Due to the collection of electrons by dust grains the electron energy can increase to an unusual level, much more than in electronegative gases, leading to highly efficient plasmas for radical production and film technologies.[6] Beside the electron temperature the electron density is also strongly affected in the presence of grains. Usually the electron density decreases with an increase of particle density or particle size. The most obvious phenomenon that is correlated with the formation of particles is a change of the light which is emitted from the discharge. The intensity as well as the spatial distribution of the emitted light are drastically changing when particles are formed in the discharge.[8,9]

In order to control the properties of complex plasmas a theoretical understanding of the interplay between particle formation and plasma parameters is crucial. Most of the theoretical studies on dusty plasmas were devoted to the study of wave propagation, dust charging, crystal and void formation.[3,10] However, the important questions concerning the effect of dust grains on power absorption and sheath formation in complex plasmas are not well studied. Boeuf *et al.*[11,12] developed a particle-in-cell Monte Carlo code and a rather complicated hydrodynamical model for dusty plasmas. Using these models they showed that in dusty plasmas the rf power is absorbed mainly in the bulk plasma. In dust-free plasmas the power is absorbed mainly in the sheaths near the plasma walls. (However, Belenguer *et al.*[12] did not explain the reason for the differences in the power absorption in dust-free and complex plasmas.)

In this article we study the response of a capacitively coupled $Ar-C_2H_2$ discharge to the formation of dust particles both experimentally and theoretically. We present the results of measurements of the intensity and the spatial dis-

a)Author to whom correspondence should be addressed. Electronic mail: idenysenko@yahoo.com

tribution of the emitted light, the line width of the fast component of H_α line and of the electron density during the particle growth.

To understand—at least qualitatively—the phenomena observed in capacitively coupled dusty discharges, a simple one-dimensional (1D) discharge model is developed. Using the model we analyze the changes in the power absorption, the electron and ion densities, the electron temperature, the current flowing across the discharge plates, the rf electric field, and in the spatial distributions of the argon atoms in an excited state during the growth of the particles. We also study the effects of dust grains on the sheath size and on the energy of positive ions bombarding the electrodes. The results of calculations are compared with available experimental data.

The article is organized as follows. The experimental setup and the experiment details are described in Secs. II and III. Section IV describes the theoretical model of the plasma. The theoretical results are presented, discussed and compared with experimental data in Sec. V. Concluding remarks are given in Sec. VI.

II. EXPERIMENTAL SETUP

The investigations were performed in a radio frequency (rf) capacitively coupled parallel plate reactor working at 13.56 MHz.[9] The electrode system consists of plane, stainless steel electrodes 30 cm in diameter and separated by 8 cm. The reactor was operated at room temperature, with a mixture of acetylene and argon. The continuous gas flow of 8 sccm for argon and 0.5 sccm for acetylene was controlled with mass flow controllers. The total gas pressure was about 0.1 mbar. The gas residence time was approximately 1 min. The applied rf power was 15–50 W measured before the match box.

The emission spectroscopy measurements were performed by the use of an Acton Research monochromator/spectrograph with a Czerny-Turner mount. The 750 mm focal length monochromator/spectrograph had a reciprocal linear dispersion of 0.74 nm mm^{-1} with a 1800 g mm^{-1} grating. The spectroscopic data were collected by a 1024 $\times$256 pixel format, front illuminated inductively coupled charge device camera from Princeton Instruments. The resolution power of our spectroscopic system was 0.06 nm or 3 pixels with a 10 μm entrance slit width. All data presented here were obtained by observing the emission at 90° from the central axis of the electrodes, i.e., parallel to the electrode surfaces. The interelectrode space was imaged onto the 3 mm high, 10 μm wide entrance slit by the system of optical mirrors and lenses. The specially designed imaging optics of the spectrograph allowed us to measure spatially resolved optical emission. The signal-to-noise ratio was improved by averaging 50 frames for one spectrum. The exposition time for one frame was 1 s. The spectra were collected in a 1 min interval, enabling us to follow the time development of the spectral emission.

For the measurement of the electron density a microwave method was applied. In principle, two variants of the microwave method can be distinguished: microwave interferometry and the microwave cavity resonance technique.[13] Both methods had been applied in the past for the measurements of the electron density in dusty plasmas.[13] In the present investigation the (line of sight averaged) electron density was measured by means of a superheterodyne microwave interferometer working at a 1 cm wavelength.

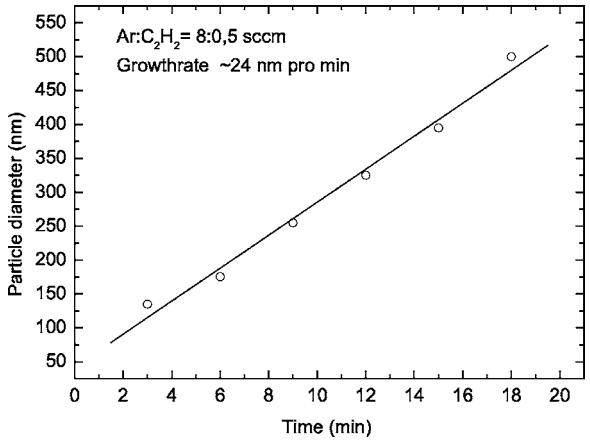

FIG. 1. Diameter of the particles as a function of time.

Laser light scattering measurements necessary for tracing the formation of dust particles have been performed by means of a He–Ne laser. The size and the growth rate of the nanoparticles have been determined from particles collected from the plasma during their growth. The particles were collected by means of a specially designed particle collector working with a cooled surface (using the effect of thermophoresis). Their size was determined by means of scanning electron microscopy.

III. EXPERIMENTAL RESULTS

A. Formation process and particle characteristics

The formation of carbonaceous dust particles in the plasma bulk and their growth is an often described phenomenon (see, e.g., Ref. 14) although some details are not completely understood. In principal there are two pathways leading to the formation of particles—homogeneous and heterogeneous growth. In our work we are interested in the case of homogeneous growth, where dust particle formation comes from gas-phase polymerization processes. As described by Perrin in Ref. 14, dust nuclei are formed after the initial growth of primary clusters. Once the particles have reached a sufficient size they become negatively charged and are therefore confined in the positive plasma potential. These negatively charged nanoparticles grow further by condensation of monomer neutrals, ions and radicals (accretion). Scanning electron microscope (SEM) pictures of particles collected in our discharge reveal that the particles are nearly spherical with a typical cauliflower shape. A more detailed analysis of the SEM pictures shows that the particles grow nearly monodisperse, i.e., their size distribution is very narrow. The size of the particles during this accretion phase is depicted in Fig. 1 as a function of time. The experimental results show that the particle diameter increases during this period linearly in time with a growth speed of approximately

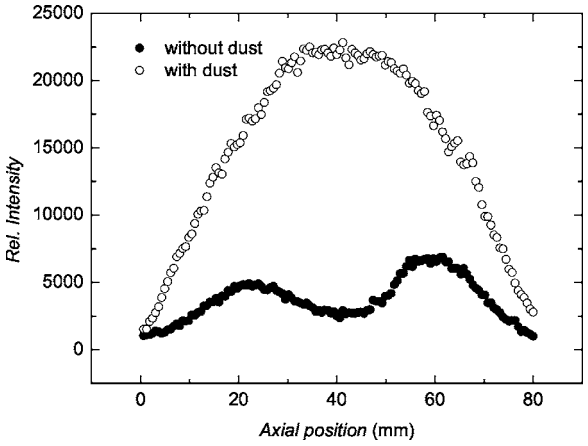

FIG. 2. Spatial profiles of the light emitted from the discharge. The electrodes are located at $z=0$ and $z=80$ mm. The closed cycles present measurements performed directly after the discharge ignition (without dust) and the open cycles present measurements performed after the dust appearance.

24 nm/min. The maximum size that the particles reach for our experimental conditions is approximately 550 nm. When the particles reach this critical size they are pushed out of the discharge and a new growth cycle starts. As a consequence the formation of particles exhibits a periodical behavior.[15]

The periodicity can be explained by the effect of different forces (the electric, ion, and neutral drag, and gravitational forces, and thermothoresis[7]) on the dust particles. The electric force is a confining force.[7] All the other forces are accelerating the dust particles outside the plasma. All the forces increase with an increase of the dust particle radius. As soon as the particles reach a critical size the forces, accelerating the dust particles to plasma walls, dominate over the confining electric force, and the particles are dragged out of plasma bulk.

B. The response of the plasma to the growth of particles

It is well known that the presence of dust particles can influence the plasma parameters to a great extent. Several investigations in silane[16] as well as in hydrocarbon rf plasmas[17] showed, e.g., that the formation of particles changes drastically the electrical properties of the discharge.

The first obvious change in the plasma properties that we could observe when dust particles start to form is the change in the light emitted from the plasma bulk. Figure 2 shows the spatial profile of the emitted light—integrated over the line of sight—for two different times [obtained 0.5 min (without dust) and 20 min after the discharge was switched on (just before the end of the dust growth cycle)]. The results show that the intensity of the light is continuously increasing during the growth of the particles. The intensity coming from the center of the discharge—integrated over the line of sight—is increasing by a factor of approximately 10. At the same time the shape of the spatial profile is changing too. In the beginning of the experiment the light intensity exhibits two pronounced maxima located near the electrodes. These maxima are slowly diminishing during the growth of the particles and about 20 min after the ignition of the discharge

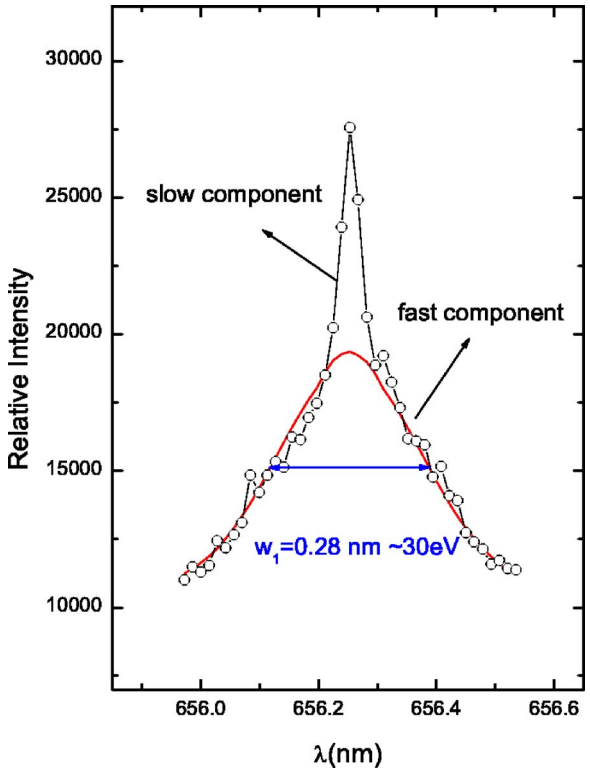

FIG. 3. The line profile of the H_α line of atomic hydrogen can be written as a sum of two Gauss functions: one Gaussian with a rather large line w_1 width and one Gaussian with a much smaller line width w_2.

they had disappeared completely. At this time the light intensity exhibits clearly a maximum located in the midplane between the two electrodes.

The spectroscopic investigation of the profile of the H_α line of atomic hydrogen revealed another phenomenon.[9] The analysis of the line profile of the H_α line shows that it can be written as a sum of two Gauss functions: one Gaussian with a rather large line w_1 width and one Gaussian with a much smaller line width w_2 (see Fig. 3):

$$y = \frac{A_1}{w_1\sqrt{\pi/2}} e^{-2(\lambda-\lambda_0)^2/w_1^2} + \frac{A_2}{w_2\sqrt{\pi/2}} e^{-2(\lambda-\lambda_0)^2/w_2^2}.$$

The central wavelength λ_0 is given by the wavelength of the Balmer alpha line ($\lambda_0=656.3$ nm), the constants A_1, A_2, w_1 and w_2 can be obtained by fitting the experimental results to the expression given previously. The experimental results show that the line width w_1 is changing due to the presence of particles inside the discharge. As long as the discharge is dust free the line profile of the H_α line exhibits a strong Doppler broadened component indicating the presence of fast H atoms. In the dust-free case the Doppler width w_1 of this fast/broad component corresponds to an average kinetic energy of the fast hydrogen atoms of about 30 eV. One source of these fast hydrogen atoms are surfaces that are exposed to the plasma: due to the dissociation of fast molecular H_2^+ ions that are impinging on the surface, due to the neutralization and subsequent reflection of fast H ions that are hitting the surface or due the ejection of adsorbed hydrogen atoms as a result of ion-surface collisions (see,

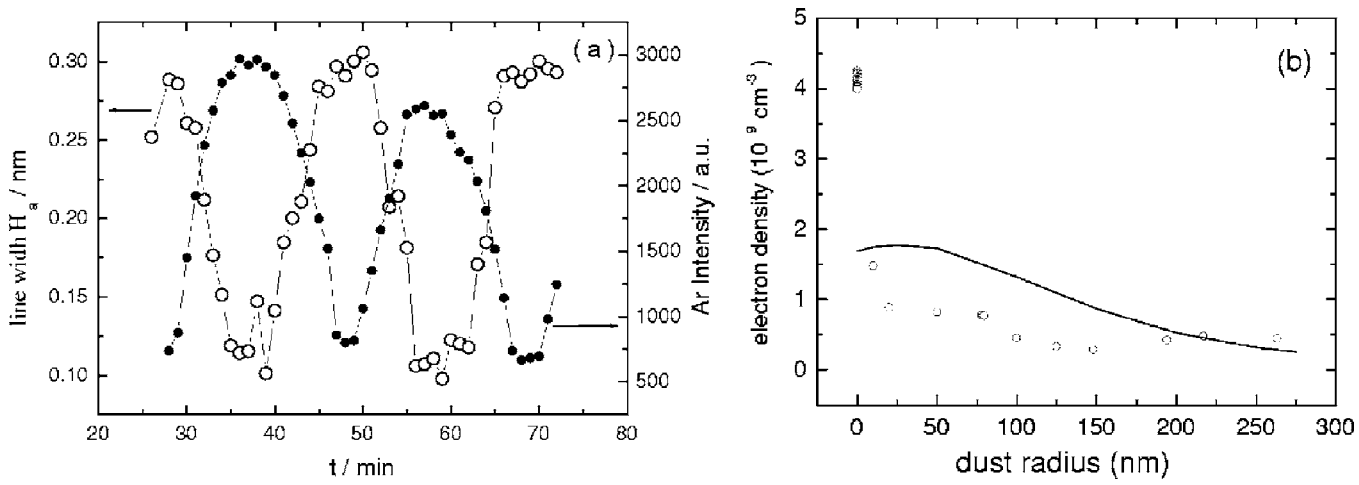

FIG. 4. (a) Line width of the fast/broad component of the H_α line and intensity of the Ar I line as a function of time. The dust particles are disappearing from the discharge at $t \approx 28$, 49, and 70 min. (b) Electron density as a function of the dust radius. The cycles present measurements and solid curve is the spatially averaged electron density obtained from the model.

e.g., Ref. 9, and references therein). Independent from the detailed mechanism leading to the production of fast H atoms it is clear that finally energetic ions are responsible for this effect, ions that get their energy in the sheath. The crucial result in the observations was that the broadened part of the line profile diminished in the presence of the dust particles. This effect underlines the fact that the energy that the ions bombard the electrodes decreases during the growth process of the particles. As soon as the particles are disappearing at the end of the growth cycle the H_α line again exhibits a strong Doppler broadened part. Figure 4(a) presents the temporal behavior of the line width of the fast component of H_α line in comparison with the temporal behavior of the intensity of the Ar I line at 660.45 nm. Both values are changing during the particle growth, but in an opposite way. The line width of the fast component of the H_α line is decreasing during the growth of the particles whereas the intensity of the Ar I line is increasing.

The line of sight averaged electron density was measured by means of a 1 cm microwave interferometer with an error of approximately 30%. Figure 4(b) shows the variation of the averaged electron density during the particle growth. One can see from Fig. 4(b) that the electron density decreases with an increase of a_d. The decrease of the electron density is probably one of the most fundamental changes that are induced by the presence of particles and can be explained (qualitatively) very easily with the negative charging of the particles. The other fundamental response of the plasma to the formation of particles concerns the electron temperature. In contrast to the electron density the electron temperature *increases* due to the formation of particles. The reason for this behavior can be explained (qualitatively) also very easily in the frame of a rather simple picture. The particles inside the discharge volume act as recombination centers, i.e., electrons and ions impinging on the particles can recombine there to form neutral atoms or molecules. In order to maintain the discharge this increase of the loss rate of electrons and ions has to be compensated by a corresponding increase of the production rate. For the usual case that the main source for the production of electrons and ions is electron impact ionization this is guaranteed by an increase of the electron temperature. In the frame of a simple corona model the intensity $I_{n\to m}$ of a spectral line (corresponding to a transition from level n to level m) is given by the relation:

$$I_{n\to m} = n_0 n_e \frac{A_{nm}}{\Sigma_{j<n} A_{nj}} \langle \sigma v \rangle. \tag{1}$$

Here n_0 is the ground state density of the argon atoms, n_e is the electron density, A_{nm} is the transition probability from level n to level m and $\langle \sigma v \rangle$ is the rate coefficient for electron impact excitation from the ground state to level n. The ground state density is approximately equal to the neutral gas density (of argon) and thus independent from the formation of particles. As the electron density drops down the increase of the light intensity (see Fig. 2) indicates the increase of the rate coefficient $\langle \sigma v \rangle$, i.e., the increase of the electron temperature.

The increase of the electron temperature/light intensity and the decrease of the electron density are rather general mechanisms (i.e., they can be observed for several types of discharges) and can be explained in the frame of rather simple models. The spatial distribution of the emitted light and the changes of the line profile of the H_α line (which is related to the sheath properties) need more theoretical effort to be understood.

IV. THE THEORETICAL MODEL

The influence of dust particles on the properties of an $Ar-C_2H_2$ rf plasma is also studied theoretically using a 1D fluid model. The study is carried out for parameters close to that in the experiment.

A. Main assumptions of the model

In the model we make some assumptions to simplify the analysis. All the assumptions were applied before in studies of dust-free capacitively coupled rf plasmas[18] and dusty

plasmas.[19] First, as the height of the discharge l is smaller than its radius, we assume that all the plasma parameters depend only on the coordinate z perpendicular to the steel electrodes of area A. The discharge is considered to be symmetric and composed of a bulk plasma region of thickness l_p separated from the electrodes by two sheaths, each having the time-averaged thickness $s_m=(l-l_p)/2$. A sinusoidal current $I_{rf}(t)=I_1 \sin(\omega t)$ (where $\omega=2\pi\times 13.56$ MHz and I_1 is the current amplitude) flows across the discharge plates, and the current is independent on z. The plasma is composed of electrons, singly charged positive ions, and negatively charged dust particles. In the experiment the Ar input is 40 times larger than that of C_2H_2. Therefore, we shall assume that Ar^+ is the dominant ion in the discharge. The effect of C_2H_2 molecules on the discharge properties is taking into account only in the energy balance equation. For the inelastic electron-C_2H_2 collisions three vibrational excitations with the threshold energies 0.09, 0.255, and 0.407 eV[20] have been accounted for. For the inelastic electron-Ar collisions we have taken into account the excitations to the $4s$ and $4p$ states. Stepwise ionization and excitation processes are neglected. It is assumed that the electron and ion energy distributions are Maxwellian with the temperatures T_e and T_i, respectively. The ions and neutrals are taken to be at room temperature (300 K). In the model we assume that the dust particles are uniformly distributed along the z axis in the center part of the discharge (at $-l_p/2+0.5$ cm$\leqslant z\leqslant l_p/2-0.5$ cm, where $z=0$ corresponds to the plasma midplane), and that the dust density drops linearly to zero at the plasma-sheath boundary. It is assumed that the dust density n_d in the discharge center is independent from the particle radius a_d and is equal to 10^7 cm^{-3}. The dust charge and the dust surface potential are calculated using the orbital motion limited approximation theory.[7] We also assume that size dispersion of the dust grains is negligible. As the dust particles are negatively charged, it is assumed that they are absent in the sheaths. Therefore, to study the sheath properties we apply the sheath theories previously developed for dust-free plasmas.[18] The bulk plasma is assumed to be quasineutral. We also assume that the total power P_{tot} transferred to the electrons per unit area in the discharge is fixed and

$$P_{tot}=P_{Ohmb}+2P_{sh}, \tag{2}$$

where P_{Ohmb} and P_{sh} are the power transferred to the electrons per unit area in the bulk plasma and one sheath, respectively. In the calculations we used $P_{tot}=0.02$ W/cm^2 that in the experiment. The power transferred to the electrons in the sheath is due to Ohmic heating and due to stochastic heating, but in the bulk plasma it is only due to Ohmic heating.[18]

B. The model equations for the bulk plasma

The time-averaged charged species concentrations and the electron temperature T_e in the quasineutral bulk plasma can be described using the following electron, ion, and energy balance equations:

$$\partial j_e/\partial z=\nu^j n_e-\nu_{ed}^c n_e, \tag{3}$$

$$\partial j_i/\partial z=\nu^j n_e-\nu_{id}^c n_i, \tag{4}$$

$$\partial q_e/\partial z=P_{in}-I_c, \tag{5}$$

where n_i is the ion density, ν^j is the ionization frequency, ν_{ed}^c and ν_{id}^c are the electron and ion collection frequencies, respectively. P_{in} is the Ohmic heating, and I_c is the power per unit volume lost in collisions. In the bulk plasma region $n_e/n_i\approx\nu_{id}^c/\nu_{ed}^c$ and $\nu_{ed}^c=\pi a_d^2 n_d(n_i/n_e)\bar{u}_i(1+2e^2|Z_d|/a_d m_i \bar{u}_i^2)$,[19] where Z_d is the dust charge. $\bar{u}_i=\sqrt{8k_BT_i/\pi m_i+u_i^2}$, u_i and m_i are the ion drift velocity and the ion mass, respectively, and k_B is the Boltzmann constant.

The electron flux j_e, the ion flux j_i and the electron heat flux q_e can be expressed in terms of three unknowns n_e, n_i and T_e:

$$j_e\approx-\mu_e n_e E_{amb}-D_e\nabla n_e, \tag{6}$$

$$j_i\approx\mu_i n_i E_{amb}-D_i\nabla n_i, \tag{7}$$

$$q_e=2.5k_BT_e j_e-k_B^2(2.5-(T_e/\nu_e)\partial\nu_e/\partial T_e)nT_e\nabla T_e/m_e\nu_e. \tag{8}$$

Here $\mu_e=e/m_e\nu_e$, $\mu_i=2e/m_i\nu_i$, $D_i=k_BT_i\mu_i/e$, $D_e=k_BT_e\mu_e/e$, $\nu_e=\nu_{en}+\nu_{ed}$, $\nu_i=\nu_{in}+\nu_{id}$, $\nu_{en}(\nu_{in})$, and $\nu_{ed}(\nu_{id})$ are the electron-neutral (ion-neutral) and electron-dust (ion-dust) momentum-transfer frequencies, respectively and E_{amb} is the ambipolar electric field. In Eq. (8) it is accounted for that ν_e is a function of the electron temperature.[21]

In the bulk plasma region $j_e\approx j_i$, and the ambipolar electric field is determined by

$$E_{amb}=\frac{D_i\nabla n_i-D_e\nabla n_e}{\mu_i n_i+\mu_e n_e}.$$

Taking into account the expression for E_{amb} from Eq. (6) we obtain

$$j_e\approx\frac{-\mu_e n_e D_i\nabla n_i-\mu_i n_i D_e\nabla n_e}{\mu_i n_i+\mu_e n_e}. \tag{9}$$

In the model it is assumed that the bulk plasma is quasineutral

$$n_e+n_d|Z_d|=n_i. \tag{10}$$

From (10) it follows that the ion density depends on n_e and Z_d. To calculate the dust charge we assume that there is no net current on the dust grain, i.e.,

$$I_i=I_e,$$

where I_i and I_e are the ion and electron currents on the dust grain, respectively. In the orbit motion limited approximation the ion current is given by

$$I_i=\pi a_d^2 e n_i\bar{u}_i[1+2e^2|Z_d|/(a_d m_i\bar{u}_i^2)].$$

The electron grain current is approximated by

$$I_e = \pi a_d^2 e n_e \sqrt{\frac{8k_B T_e}{\pi m_e}} \exp\left(\frac{-e^2|Z_d|}{a_d k_B T_e}\right).$$

For low rf frequencies $\omega \ll \nu_e, \omega_{pe}$ (where ω_{pe} is the electron plasma frequency) the Ohmic heating in Eq. (5) is [see Eqs. (4.2.30) and (11.1.25) in Ref. 18]

$$P_{in} = 0.5 J_1^2 m_e \nu_e / (e^2 n_e), \tag{11}$$

where $J_1 = I_1/A$. In the case the power transferred to the electrons per unit area in the bulk plasma

$$P_{\text{Ohmb}} = \int_{-l_p/2}^{l_p/2} P_{in} dz. \tag{12}$$

The power per unit volume lost in collisions in Eq. (5) is $I_c \approx n_e(\Sigma_j \nu_j U^j + \nu^i U^i) + n_d S_{ed}$, where ν_j is the excitation frequency from the ground state to level j with a threshold energy U^j, and U^i the ionization energy. S_{ed} is the power lost in electron-dust collisions per dust grain. It can be found from Ref. 22:

$$S_{ed} \approx \pi a_d^2 n_e \int_{-e\Phi_s}^{\infty} u^{3/2}(1 + e\Phi_s/u)\sqrt{2u/m_e} F_0 du,$$

where $\Phi_s = eZ_d/a_d$ is the dust surface potential, u and F_0 are the electron energy and energy distribution function, respectively. For Maxwellian electrons with $F_0 = (2/\sqrt{\pi}) \times (k_B T_e)^{-3/2} \exp(-u/k_B T_e)$ we have

$$S_{ed} \approx \pi a_d^2 n_e \frac{2^{3/2}\sqrt{k_B T_e}}{\sqrt{\pi m_e}} \exp(e\Phi_s/k_B T_e)[2k_B T_e - e\Phi_s].$$

Equations (3), (5), and (8)–(10) describing the spatial distributions of n_e, n_i, T_e, q_e, and j_e in the bulk plasma region have to be supplemented by boundary conditions. Here, we assume that at the bulk plasma-sheath boundary the ion drift velocity is equal to the Bohm velocity $u_B = (k_B T_e/m_i)^{0.5}$ and $\partial T_e/\partial z = 0$. Because of the discharge symmetry, the electron flux and electron heat flux must vanish at $x = 0$.

To calculate n_e, n_i, T_e, q_e, and j_e from (3), (5), and (8)–(10), it is necessary to know the thickness of the bulk plasma region l_p and the power transferred to the electrons in the bulk plasma P_{Ohmb}. The thickness of the bulk plasma region depends on the sheath size: $l_p = l - 2s_m$.

C. The model equations for the sheath region

The sheath thickness in the collisional rf plasma is:[23]

$$s_m = 1.95 H s_0, \tag{13}$$

where $H = [2\lambda_i s_0/(\pi^2 \lambda_{De}^2)]^{1/2}$ and $s_0 = J_1/(e\omega n_{es})$. Here λ_i is the ion mean free path, which is assumed to be constant in the bulk plasma and the sheaths. λ_{De} and n_{es} are the electron Debye length and the electron density at the bulk plasma-sheath boundary, respectively. The power P_{sh} transferred to the electrons per unit area in the sheath is due to Ohmic heating P_{Ohmsh} and due to stochastic heating P_{stoc}[24], i.e., $P_{\text{sh}} = P_{\text{Ohmsh}} + P_{\text{stoc}}$. The Ohmic heating in the sheaths can be found from the results presented in Ref. 23. The instantaneous Ohmic power per unit area dissipated in one sheath is[24]

$$S(t) = \int_0^s J_1^2 m_e \nu_e / (e^2 n_i(s)) \sin^2(\omega t) ds, \tag{14}$$

where $s(\phi)$ is the instantaneous position of the oscillating electron sheath edge at the phase $\phi = \omega t$. Writing $ds/n_i(s) = (ds/d\phi)d\phi/n_i(\phi)$ and using Eqs. (11) and (12) in Ref. 23 to determine $ds/d\phi$ and $n_i(\phi)$, we obtain

$$S(t) = \frac{m_e \nu_e}{e} \frac{s_0 2\lambda_i}{n_{es} u_B^2 \pi m_i} J_1^2 \sin^2(\omega t) \int_0^{\omega t} \bar{E} \sin(\phi) d\phi, \tag{15}$$

where $\bar{E} = (4J_1/\omega)(\sin\phi - \phi\cos\phi)$.

Averaging Eq. (15) over the phase interval $\omega t = (0, \pi)$, we obtain

$$P_{\text{Ohmsh}} = \bar{S} = \frac{3 m_e \nu_e J_1^3 s_0 \lambda_i}{4 e n_{es} k_B T_{es} \omega}, \tag{16}$$

where T_{es} is the electron temperature at the bulk plasma-sheath boundary. The power per unit area dissipated in one sheath due to stochastic heating is [see Eq. (36) in Ref. 23]

$$P_{\text{stoc}} = \frac{1}{2}\frac{J_1^2}{G_s}, \tag{17}$$

where $G_s = 1.02 e^2 n_{es}/(H m_e v_{T_e})$ with $v_{T_e} = \sqrt{8k_B T_e/\pi m_e}$.

One can also estimate the average energy E_{ic} that the ions bombard the electrodes. The energy is [see Eq. (11.2.57) in Ref. 18]:

$$E_{ic} \approx 0.62 \bar{V} \lambda_i / s_m. \tag{18}$$

Here $\bar{V}$ is the time averaged voltage across each sheath. From Eqs. (11.2.55) and (11.2.56) in Ref. 18 it follows that $E_{ic} \propto J_1$. The average ion-bombarding energy E_{ic} is reduced below $\bar{V}$ because ion energy is lost during charge transfer and elastic collisions in the sheaths, creating fast neutrals there.[18] Independent from the detailed mechanism that is responsible for the creation of fast neutrals it is reasonable to assume that the energy of the fast neutrals is proportional to E_{ic} and consequently to J_1.

The profiles of the electron and ion densities, electron flux, electron heat flux and electron temperature in the bulk plasma are computed from Eqs. (3), (5), and (8)–(10). The computation is initialized using profiles of n_e, n_i, T_e, q_e, and j_e estimated from less accurate analytical or computational results. From the guessed bulk plasma thickness l_p and the power transferred to the electrons in the bulk plasma the profiles of n_e, n_i, T_e, q_e, and j_e are calculated from Eqs. (3), (5), and (8)–(10). Then, using the bulk plasma parameters the sheath size and P_{sh} are obtained from Eqs. (13), (16), and (17). The calculated s_m and P_{sh} values are used to find P_{Ohmb} and l_p. The cycle is repeated until the parameters become constant within a prescribed tolerance. The differential equations (3), (5), (8), and (9) are solved using a finite difference scheme based on the balanced integro-interpolation method.[25] A detailed description of the numerical method can be found in Ref. 26.

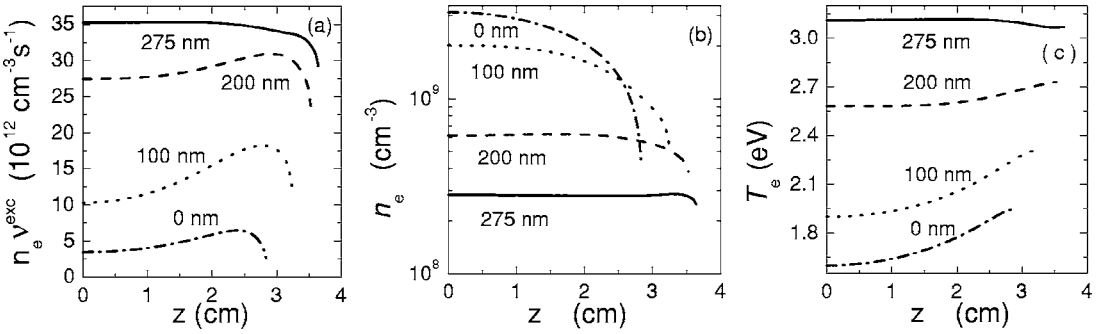

FIG. 5. (a) $n_e\nu^{\mathrm{exc}}$, (b) electron density, and (c) electron temperature profiles for $P_{\mathrm{tot}}=0.02$ W/cm^2, $p_0=0.125$ Torr, and different particle radii a_d.

V. THEORETICAL RESULTS

In this section we will use the model presented in the previous section to analyze theoretically an $Ar-C_2H_2$ rf dusty plasma for parameters that are close to that in the experiment. In the study we will vary the dust radius from 0 up to 275 nm (as in the experiment). First, we will consider how the dust particles affect the optical emission intensity (OEI) of the 660.45 nm argon line that is due to electron transitions from $4d$ to $4p$ levels in argon atoms. It is assumed that the OEI is proportional to $n_e\nu^{\mathrm{exc}}=n_e n_0\langle\sigma v\rangle$ [see Eq. (1)], where ν^{exc} is the corresponding excitation frequency for electron impact excitation from the ground state to $4d$ state. The excitation frequency is calculated using the excitation cross section for the $4d$ excited state given by Eggarter.[27]

The calculated $n_e\nu^{\mathrm{exc}}$ profiles for different a_d are shown in Fig. 5(a). The calculations are carried out for pressure $p_0=0.125$ Torr. We fixed the pressure in the calculations because at the pressure in the dust-free discharge the difference between the maximum value of $n_e\nu^{\mathrm{exc}}$ and the value at $z=0$ is about a factor of 2 (about the same as the difference in the corresponding optical emission intensities in the experiment). For $p_0=0.076$ Torr the difference between the maximum value and the value at $z=0$ is approximately 5%. From Fig. 5(a) one can see that $n_e\nu^{\mathrm{exc}}$ increases with increase of the dust radius. Besides, the growth of a_d is accompanied by an increase of $n_e\nu^{\mathrm{exc}}$ at $z=0$ with respect of the maximum value. For a particle radius of 275 nm the maximum of $n_e\nu^{\mathrm{exc}}$ is located in the discharge center, whereas for smaller radii the maxima are located near the electrodes. Both results are in agreement with the experimental results as they are depicted in Fig. 2. The variation of the $n_e\nu^{\mathrm{exc}}$ profiles with increasing particle radius a_d is due to changes in the electron density and temperature profiles. Therefore, we will discuss now the changes in the electron density and temperature profiles that are induced by the presence of dust particles.

Figure 5(b) shows the electron density distributions for different particle radii a_d. In the dust-free plasma or for small values of a_d the electron density profile is close to the well-known cosinus profile. With the increase of a_d the profile flattens and is almost uniform in the main part of the discharge for large particle radii, which is in agreement with the results of Belenguer *et al.* (Ref. 12, Fig. 9). In our opinion, the n_e distribution becomes more uniform for large dust sizes because the electron recombination on the dust grains dominates over the electron diffusion losses to plasma walls. The spatial distribution of the dust particles is for large values of a_d the main factor affecting the n_e profile. Because of the nearly uniform n_e distribution for relatively large values of a_d the power absorption in the bulk plasma is also nearly uniform [see Eq. (11)], and as a result, T_e also becomes more uniform [Fig. 5(c)].

Concerning the behavior of $n_e\nu^{\mathrm{exc}}$ one can finally conclude: $n_e\nu^{\mathrm{exc}}$ depends on n_e and T_e, and when n_e and T_e are uniform in the bulk plasma $n_e\nu^{\mathrm{exc}}$ is also nearly uniform [see Fig. 5(a)].

Compare the calculated spatially averaged electron density $\langle n_e\rangle$ with the electron density obtained in the experiment. In Fig. 4(b) the dependence of $\langle n_e\rangle$ on a_d is shown. One can see that at $a_d<150$ nm both the measured and calculated densities decrease with an increase of a_d. Meantime, in the range 150 nm$<a_d<$220 nm the measured electron density slightly increases with a_d increase whereas the calculated $\langle n_e\rangle$ decreases. The difference in the electron densities may be due to some simplifications in the model as well as errors (about 30%) at the electron density measurements.

Consider using the theoretical model how the dust particles affect the average energy E_{ic} that the ions bombard the electrodes. As it was mentioned in the previous section the average energy depends on J_1 [see discussion after Eq. (18)]. The dependence of J_1 (constant through the plasma slab) on the particle radius a_d is presented in Fig. 6(a). J_1 shows a similar behavior as the calculated averaged electron density, it is also decreasing with increasing particle radius. The decrease of J_1 can be explained if we take into account that $P_{in}\propto J_1^2/n_e$. For a constant power P_{tot} one can expect that J_1^2 varies like $\langle n_e\rangle$. From the theory it follows that the energy that the ions bombard the electrodes decreases with an increase of a_d because of the decrease of J_1. As a result of the E_{ic} decrease, the line width of the fast component of the H_α line decreases in the presence of the dust particles [see Fig. 4(a)].

Now we will analyze how the dust particles affect the rf electric field amplitude E_{rf}. For the conditions of the experiment ($\omega\ll\nu_e,\omega_{pe}$) the rf electric field can be found from the relation:[18]

$$E_{\mathrm{rf}}\approx J_1/\sigma_{\mathrm{dc}},$$

where $\sigma_{\mathrm{dc}}\approx e^2 n_e/(m_e\nu_e)$.

The profiles of E_{rf} for different a_d are shown in Fig. 6(b). One can see from Fig. 6(b) that with an increase of a_d the rf

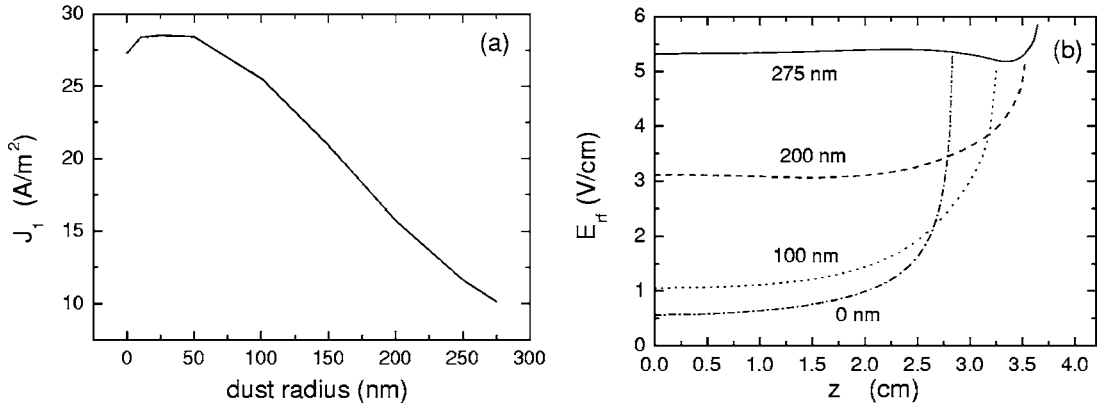

FIG. 6. (a) The dependence of J_1 on the dust radius and (b) the E_{rf} profiles for different a_d for parameters corresponding to those in Fig. 5.

electric field in the central part of the discharge becomes more uniform and its magnitude increases, that agrees with the results presented in Ref. 28. In our opinion, the variation of the E_{rf} spatial distribution is due to the flattening the n_e profile [see Fig. 5(b)]. Magnitude of the rf electric field increases because of the decrease of $\langle n_e \rangle$ [see Fig. 4(b)].

The dust particles also affect the power absorption in the discharge. The dependencies of $P_{\mathrm{Ohmb}}/P_{\mathrm{tot}}$, $2P_{\mathrm{stoc}}/P_{\mathrm{tot}}$, and $2P_{\mathrm{Ohmsh}}/P_{\mathrm{tot}}$ on a_d are shown in Fig. 7(a). One can see from Fig. 7(a) that in the dust-free plasma approximately 70% of the input power is absorbed in the sheaths whereas only 30% is absorbed in the bulk plasma. With the increase of the particle radius a_d the power absorption in the sheaths decreases, whereas the power absorption in the bulk increases. For a particle radius of a_d=275 nm approximately 90% of the input power is absorbed in the bulk plasma. The decrease of the power absorption in the sheaths with increasing a_d is due to the dependencies of P_{Ohmsh} (16) and P_{stoc} (17) on J_1, T_{es} and n_{es}. [The dependence of n_{es} on a_d is shown in Fig. 7(b).] As

$$P_{\mathrm{Ohmsh}} \propto J_1^4/(n_{es}^2 T_{es})$$

and

$$P_{\mathrm{stoc}} \propto J_1^{5/2}/n_{es}$$

the power absorption in the sheath decreases with increasing a_d, because J_1 decreases and T_{es} increases.

It is interesting to note that the sheath size decreases with increasing particle radius a_d [Fig. 7(b)]. A similar phenomenon can be found in electronegative plasmas where the presence of negative ions induces a sheath contraction.[29] The decrease of s_m with an increase of a_d is due to the dependence of the sheath size on J_1, T_{es} and n_{es} [see Eq. (13)]:

$$s_m \sim J_1^{3/2}/(n_{es} T_{es}^{1/2}).$$

As n_{es} does not change strongly with increasing a_d [Fig. 7(b)], s_m decreases substantially due to the increase of T_{es} and the decrease of J_1.

VI. SUMMARY

Thus the existence of particles can drastically change the properties of a discharge. The electron temperature, the electron density, the density of excited states, the spatial profiles

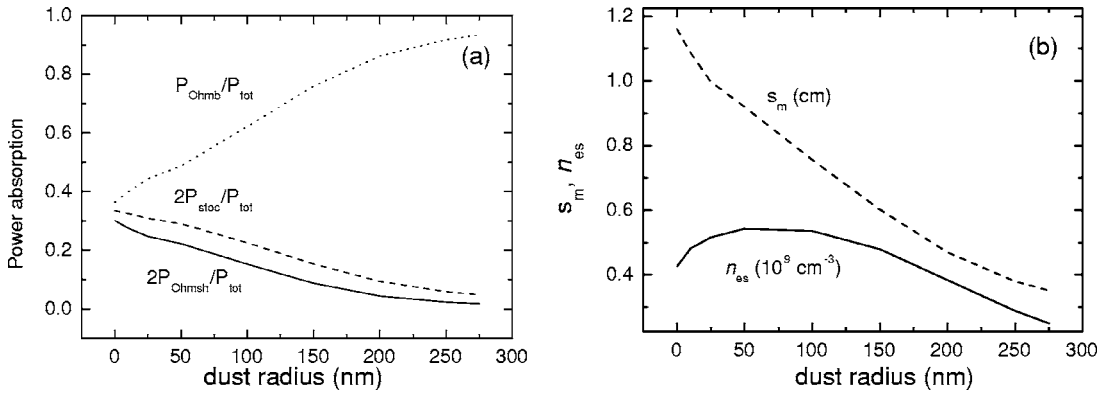

FIG. 7. (a) Dependencies of $P_{\mathrm{Ohmb}}/P_{\mathrm{tot}}$, $2P_{\mathrm{Ohmsh}}/P_{\mathrm{tot}}$, and $2P_{\mathrm{stoc}}/P_{\mathrm{tot}}$ on the particle radius a_d. (b) Sheath size and boundary electron density n_{es} as a function of the particle radius for parameters corresponding to those in Fig. 5.

of these values, the power absorption, the sheath properties, etc.: all these parameters are changing due to the existence of particles inside the discharge.

Even without using sophisticated diagnostics, the light emitted from the discharge is a simple indicator for the presence of dust. Especially for a capacitively coupled discharge the emitted light exhibits some typical changes as soon as dust particles are formed inside the plasma volume. The intensity as well as the spatial distribution of the emitted light are drastically changing during the growth of the particles. Even the line profile (of the Balmer alpha line of atomic hydrogen) is affected by the presence of particles.

It was the aim of this paper to explain the observations within the frame of a rather simple model, that is based on a fluid description of the plasma. The theoretical results show that the model is able to explain the experimental observations: the increase of the light intensity with increasing particle radius, the flattening of the emission profile at the same time, the decrease of the electron density during the growth of the particles and the simultaneous decrease of the energy with that the ions bombard the electrodes. The decrease of the ion energy with increasing particle radius is important to explain the observations concerning the broadening of the H_α profile. An important result concerns the power absorption. For the parameters considered in this article most of the power is absorbed within the sheaths as long as the plasma is free of dust particles. With increasing particle radius more and more power is absorbed in the plasma bulk. Due to the simplicity of the model it is possible to explain the most important dependencies in a semianalytical manner. It is easy to understand that the electron density is decreasing with increasing particle radius: with increasing a_d the losses of electrons—due to recombination on the surface of the particle—are increasing too. The same argument holds for the electron temperature: it is increasing to compensate the increase in the loss rate. The electron density profile becomes more uniform for large dust radii (at roughly uniform distribution of the dust particles) because the electron recombination on the dust grains dominates over the electron losses to plasma walls. Because of the nearly uniform n_e at large a_d and of the dependence of the Ohmic heating in the bulk plasma on n_e the power absorption in the bulk plasma and the electron temperature are also nearly uniform. The current that flows across the discharge plates decreases with an increase of a_d also because of the dependence of the Ohmic heating in the bulk plasma on n_e [see Eq. (11)]. Taking into account the effects of the dust particles on the electron density and temperature and the current the relations (13) and (16)–(18) easily explain the change in the power absorption, the sheath size and the energy that the ions bombard the electrodes.

However, the model has some limits. In particular, we have assumed that the plasma is quasineutral, i.e., using the model it is impossible to study the space charge layers in the bulk of dusty plasmas.[30] The dust charge is calculated using the orbit motion limited approximation. The approximation is applicable for low neutral gas pressures[31] and for dust radii $a_d < 1\ \mu$m.[7,32,33] Using the model it is also impossible to explain why the particles stop to grow and disappear from the discharge at $a_d > 275$ nm. To explain the phenomena the forces affecting on the dust grains in the plasma have to be studied. Moreover, in the study it is assumed that the dust particles are roughly uniform distributed in the bulk plasma. In reality, the dust density distribution depends on the neutral gas pressure, temperature, as well as on the discharge volume. Light scattering experiments show that for relatively large particle radii a_d a void appears in the center of the discharge. This effect is not taken into account in our model. If we apply our model to the case when a void is in the center of the discharge the results show that $n_e \nu^{\mathrm{exc}}$ decreases in the center, i.e., in the void. We think however that this result is due to some simplifications in the model. Particularly, we assume in this study that the electron energy distribution function (EEDF) is a Maxwellian. Consequently the effect of the dust particles on the shape of the EEDF is not accounted for. This is probably not true for large dust radii or large dust concentrations.[8] At uniform plasma heating in dust-free regions the number of high-energy electrons in the EEDF is larger than that in dusty plasma regions.[34] The fairly uniform profile of n_d is relevant to dust growth in the entire reactor as in the case for the rf SiH_4 and SiH_4/Ar plasmas.[1,12] This distribution is also applicable to experiments where the particles are injected externally.[35] Meanwhile, in certain chemically active processing plasmas[36,37] and at formation of the voids in dusty plasmas[38,39] the dusts are located at the plasma periphery.

ACKNOWLEDGMENTS

One of the authors (I.D.) was supported by the Humboldt Foundation. This work was supported by DFG (SFB 591 Project Nos. B1 and B5).

[1] A. Bouchoule, "Technological impacts of dusty plasmas," in *Dusty Plasmas: Physics, Chemistry, and Technological Impacts in Plasma Processing*, edited by A. Bouchoule (Wiley, New York, 1999).
[2] E. Stoffels, W. W. Stoffels, H. Kersten, G. H. P. M. Swinkels, and G. M. W. Kroesen, Phys. Scr. **T89**, 168 (2001), and references therein.
[3] S. V. Vladimirov and K. Ostrikov, Phys. Rep. **393**, 175 (2004), and references therein.
[4] S. Veprek, S. Reiprich, and L. Shizi, Appl. Phys. Lett. **66**, 2640 (1995).
[5] Ch. Hollenstein, Plasma Phys. Controlled Fusion **42**, R93 (2000).
[6] L. Boufendi and A. Bouchoule, Plasma Sources Sci. Technol. **11**, A211 (2002), and references therein.
[7] J. P. Boeuf and C. Punset "Physics and modelling of dusty plasmas," in *Dusty Plasmas: Physics, Chemistry, and Technological Impacts in Plasma Processing*, edited by A. Bouchoule (Wiley, New York, 1999).
[8] K. Tachibana, Y. Hayashi, T. Okuno, and T. Tatsuta, Plasma Sources Sci. Technol. **3**, 314 (1994).
[9] I. Stefanovic, E. Kovacevic, J. Berndt, and J. Winter, New J. Phys. **5**, 39.1 (2003).
[10] O. Bystrenko and A. Zagorodny, Phys. Rev. E **67**, 066403 (2003).
[11] J. P. Boeuf, Phys. Rev. A **46**, 7910 (1992).
[12] Ph. Belenguer, J. Ph. Blondeau, L. Boufendi, M. Toogood, A. Plain, A. Bouchoule, C. Laure, and J. P. Boeuf, Phys. Rev. A **46**, 7923 (1992).
[13] L. Boufendi, W. Stoffels, and E. Stoffels "Diagnostics of a dusty plasma," in *Dusty Plasmas: Physics, Chemistry, and Technological Impacts in Plasma Processing*, edited by A. Bouchoule (Wiley, New York, 1999).
[14] J. Perrin "Sources and growth of particles," in *Dusty Plasmas: Physics, Chemistry, and Technological Impacts in Plasma Processing*, edited by A. Bouchoule (Wiley, New York, 1999).
[15] E. Kovacevic, I. Stefanovic, J. Berndt, and J. Winter, J. Appl. Phys. **93**, 2924 (2003).
[16] L. Boufendi, J. Gaudin, S. Huet, G. Viera, and M. Dudemaine, Appl. Phys. Lett. **79**, 4301 (2001).

[17] S. Hong, J. Bernd, and J. Winter, Plasma Sources Sci. Technol. **12**, 46 (2003).
[18] M. A. Lieberman and A. J. Lichtenberg, *Principles of Plasma Discharges and Materials Processing* (Wiley, New York, 1994).
[19] K. Ostrikov, I. B. Denysenko, S. V. Vladimirov, S. Xu, H. Sugai, and M. Y. Yu, Phys. Rev. E **67**, 056408 (2003).
[20] M. Hayashi, in *Nonequilibrium Processes in Partially Ionized Gases*, edited by M. Capitelli and J. N. Bardsley (Plenum, New York, 1990).
[21] V. E. Golant, A. P. Zhilinskii, and I. E. Sakharov, *Fundamentals of Plasma Physics* (Wiley, New York, 1980).
[22] I. Denysenko, M. Y. Yu, K. Ostrikov, and A. Smolyakov, Phys. Rev. E **70**, 046403 (2004).
[23] M. A. Lieberman, IEEE Trans. Plasma Sci. **17**, 338 (1989).
[24] G. R. Misium, A. J. Lichtenberg, and M. A. Lieberman, J. Vac. Sci. Technol. A **7**, 1007 (1989).
[25] A. N. Tichonov and A. A. Samarskii, *Partial Differential Equations of Mathematical Physics* (Holden-Day, San Francisco, 1967).
[26] N. A. Azarenkov, I. B. Denysenko, A. V. Gapon, and T. W. Johnston, Phys. Plasmas **8**, 1467 (2001).
[27] E. Eggarter, J. Chem. Phys. **62**, 833 (1975).
[28] J. Perrin, P. Molinas-Mata, and P. Belenguer, J. Phys. D **27**, 2499 (1994).
[29] J. P. Boeuf, Phys. Rev. A **36**, 2782 (1987).
[30] M. R. Akdim and W. J. Goedheer, Phys. Rev. E **67**, 066407 (2003).
[31] S. Ratynskaia, S. Khrapak, A. Zobnin, M. H. Thoma, M. Kretschmer, A. Usachev, V. Yaroshenko, R. A. Quinn, G. E. Morfill, O. Petrov, and V. Fortov, Phys. Rev. Lett. **93**, 085001 (2004).
[32] J. E. Daugherty, R. K. Porteous, M. D. Kilgore, and D. B. Graves, J. Appl. Phys. **72**, 3934 (1992).
[33] R. V. Kennedi and J. E. Allen, J. Plasma Phys. **69**, 485 (2003).
[34] I. Denysenko, M. Y. Yu, K. Ostrikov, N. A. Azarenkov, and L. Stenflo, Phys. Plasmas **11**, 4959 (2004).
[35] K. Tachibana and Y. Hayashi, Pure Appl. Chem. **68**, 1107 (1996).
[36] A. Garscadden, B. N. Ganguly, P. D. Haaland, and J. Williams, Plasma Sources Sci. Technol. **3**, 239 (1994).
[37] F. J. Gordillo-Vazquez, M. Camero, and C. Gomez-Aleixandre, Plasma Sources Sci. Technol. **15**, 42 (2006).
[38] J. Goree, G. E. Morfill, V. N. Tsytovich, and S. V. Vladimirov, Phys. Rev. E **59**, 7055 (1999).
[39] D. Samsonov and J. Goree, Phys. Rev. E **59**, 1047 (1999); IEEE Trans. Plasma Sci. **27**, 76 (1999).